Supporting Information

Multilayer nanocomposites with ultralow loadings of nanofillers exhibiting superb capacitive energy storage performance

Yu Cheng[1], Yu Feng[4], Zhongbin Pan[1]*, Peng Wang[2]*, Jinjun Liu[1], Liang Liang[4], Jinhong Yu[5], Jiwei Zhai[2], and Qing Wang[3]*

[1]School of Materials Science and Chemical Engineering, Ningbo University, Ningbo, Zhejiang 315211, China. Email: panzhongbin@163.com

[2]School of Materials Science & Engineering, Tongji University, Shanghai 201804, China.Email: wangpeng2019@tongji.edu.cn

[3]Department of Materials Science and Engineering, The Pennsylvania State University, University Park, PA 16802, USA. Email: wang@matse.psu.edu

[4]Key Laboratory of Engineering Dielectrics and Its Application, Ministry of Education, Harbin University of Science and Technology, Harbin 150080, China

[5]Key Laboratory of Marine Materials and Related Technologies, Zhejiang Key Laboratory of Marine Materials and Protective Technologies, Ningbo Institute of Materials Technology and Engineering, Chinese Academy of Sciences, Ningbo 315201, China

Experimental Section

Material. Alumina (γ-Al$_2$O$_3$, 10 nm) nanoparticles (3.6 g/cm^3) and PMMA ($\sim$350 000, 1.16 g/cm^3) pellets were purchased from Sigma-Aldrich. N, N-dimethyl-formamide (DMF, AR, 99.5%) was supplied by Shanghai Aladdin Industrial Inc. All materials were used as received.

Fabrication of single-layer nanocomposite films. The nanocomposite films were prepared via a typical solution-casting and hot-pressing method. 1g PMMA pellets were dispersed into 10 ml of DMF solvent with stirring for 12 h to obtain a homogeneous solution. The different concentrations Al$_2$O$_3$ NPs were added into homogeneous solution A after sonication for 30 min and stirred for 24 h to form a uniform and stable mixed suspension. The mixed solution was then cast onto glass plate and dried under vacuum at 60 °C for 24 h. After being peeled off from the glass plates, flexible and transparent Al$_2$O$_3$ NPs/PMMA nanocomposite films were obtained. Subsequently, the composite films were subjected to a hot-pressing process at a temperature of 150 °C and a pressure of 15 MPa for 15 min. The average thickness of nanocomposite films is around 10-15 um.

Fabrication of multilayer nanocomposite films. The multilayer nanocomposite films were prepared using layer-by-layer casting technique and hot-pressing method. 1g PMMA pellets were dispersed into 10 ml of DMF solvent with stirring for 12 h to obtain a homogeneous solution. The different concentrations Al$_2$O$_3$ NPs were added into homogeneous solution after sonication for 30 min and stirred for 24 h to form a uniform and stable mixed suspension. The mixed solution was then cast onto glass plate via layer-by-layer casting technique and dried under vacuum at 60 °C for 24 h. After being peeled off from the glass plates, flexible and transparent multilayer nanocomposite films were obtained. Subsequently, the composite films were subjected to a hot-pressing process at a

temperature of 150 °C and a pressure of 15 MPa for 15 min. The average thickness of nanocomposite films is around 10-15 um.

Characterization. The cross-sectional views of the composites were characterized using field emission scanning electron microscopy (FE-SEM). TEM images were taken using a Joel JEM-2100Finstruments. The crystalline structure of the material was obtained by X-ray diffraction (XRD) on a D8 Advance X-ray diffractometer. By sputtering a 2 mm diameter gold electrode on the surface of the PMMA-based nanocomposites using an automatic fine coater (JFC-1600, JEOL, Ltd.). Dielectric performances of composites were measured by means of an LCR meter in the frequency range from 10^2 to 10^6 Hz. The *D-E* loops and leakage-electric field (*I–V*) curves were measured with ferroelectric test system (Poly *K*, United States). Dielectric breakdown strength was measured via the electrostatic pull-down method under a DC voltage ramp of 500 V/s. The thermally stimulated depolarization current (TSDC) is determined by the Keysight B2985 electrometer. The samples were first polarized at 80°C for 40 mins under a 30 MV/m DC electric field, then rapidly cooled to 20°C and maintained for 5 minutes. Finally, the samples were heated to 150°C at a heating rate of 2 °C/min and the current was recorded.

Finite element simulation of time breakdown paths. The time breakdown paths of composite films were simulated by MATLAB and COMSOL-Multiphysics. The growth probability *p* of electric tree differentiation is expressed using the fractal medium breakdown model and percolation model,

$$p(i^{'},j^{'} - i,j) = \frac{(\phi_{i^{'},j^{'}} - \phi_{i,j} - \phi_{PMMA})^{\eta}}{\sum (\phi_{i^{'},j^{'}} - \phi_{i,j} - \phi_{PMMA})^{\eta}} + (\phi_{i^{'},j^{'}} - \phi_{i^{''},j^{''}} - \phi_{PMMA})^{\eta} - loss$$

where ϕ_{PMMA}, $\phi_{i,j}$, $\phi_{i^{'},j^{'}}$, η and $\phi_{i^{''},j^{''}}$ were the threshold electrical potential of PMMA, electrical potential of discharged point, probable point, fractal dimension and linked point, respectively. The

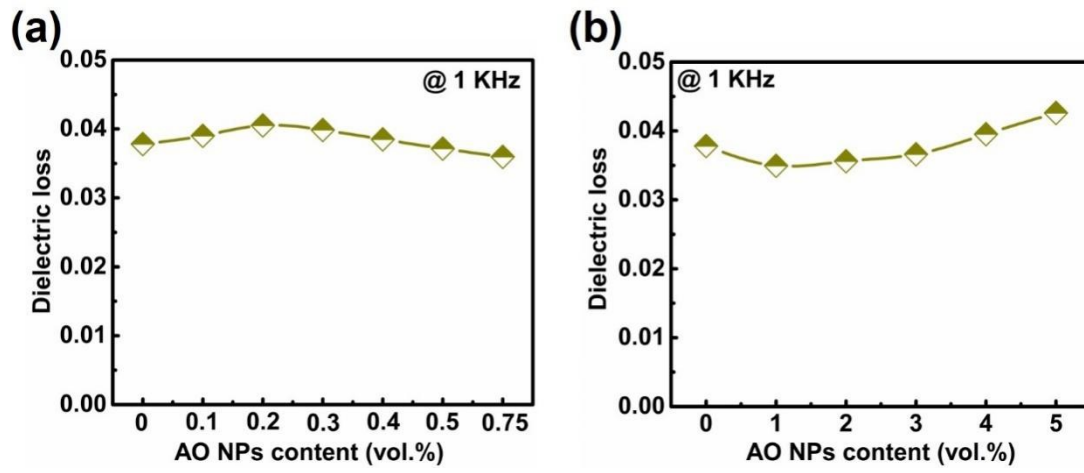*loss* represented evolve loss of tip electric tree channels.

Fig. S1 (a), (b) Dielectric loss of PMMA and the PMMA nanocomposites with different contents of
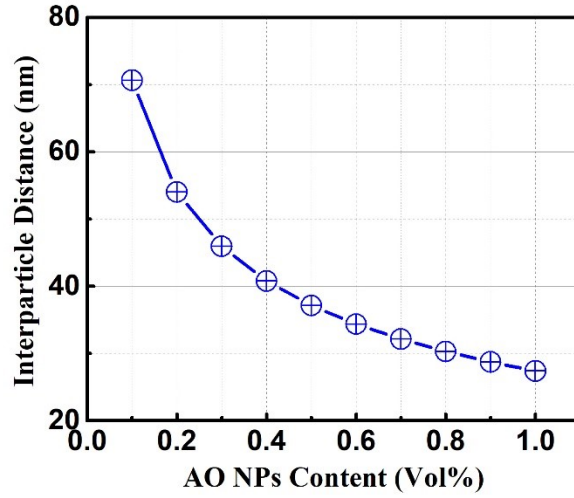
AO NPs at 1 kHz.

Fig. S2 Theoretical value of interparticle distance (*d*) as a function of AO NPs content.

The theoretical interparticle distance (*d*) in the polymer nanocomposites is determined by filler size (*D*) and filler volume fraction (*φ*), as given:

$$d = D \times \left[\left(\frac{\pi}{6\varphi} \right)^{1/3} - 1 \right]$$

According to this formula, we can calculate the *d* values in the AO NPs/PMMA nanocomposites with different AO NPs contents, as shown in Fig. R3. It is seen that *d* decreases a lot from ~70.62 nm of the nanocomposites with 0.1 vol% AO NPs to ~53.99 nm and ~45.93 nm of the ones with 0.2 vol% and 0.3 vol% AO NPs, respectively. According to Figure 2f, the experiment results of partial interparticle distance (d) is less than ~45.93 nm (theoretical value), possibly indicative of the formed overlapped interface of two adjacent fillers.
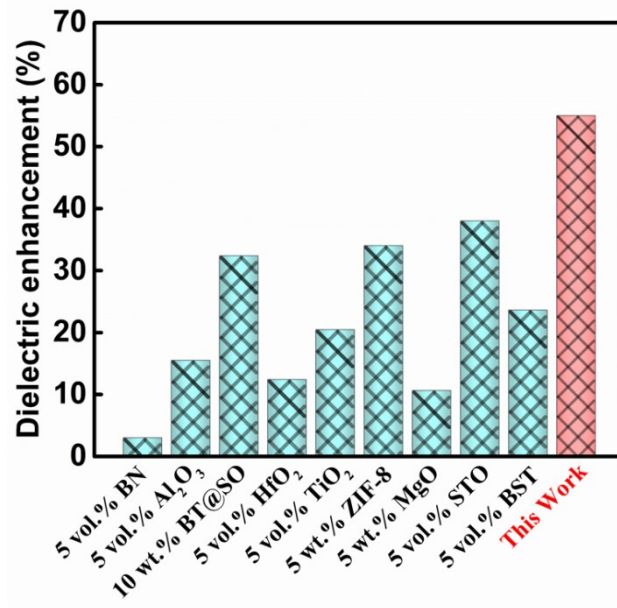
Fig. S3 Comparison of dielectric enhancement rations of nanocomposite films with this work and previous reported.[s1-s7]
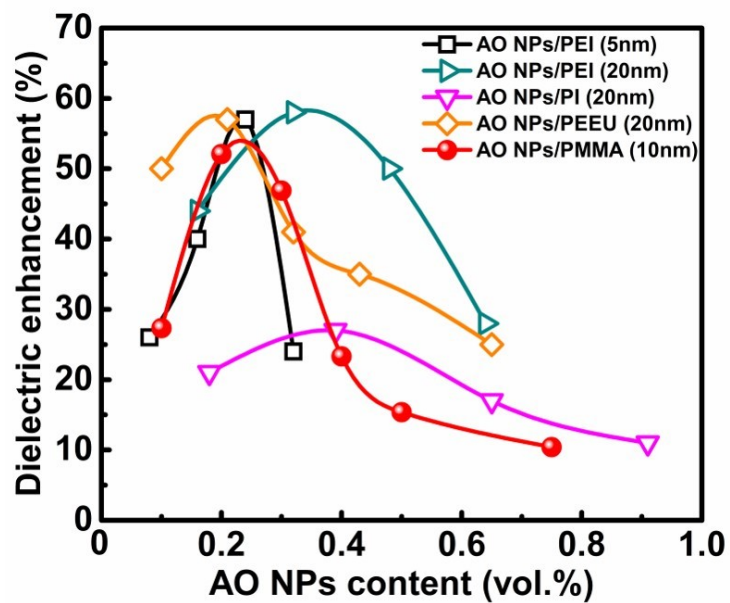
Fig. S4 Comparison with the variation of the dielectric enhancement ratios of polymer nanocomposites (AO NPs/PEI, AO NPs/PI, AO NPs/PEEU, AO NPs/PMMA) as a function of AO NPs loading.[s8-s10]

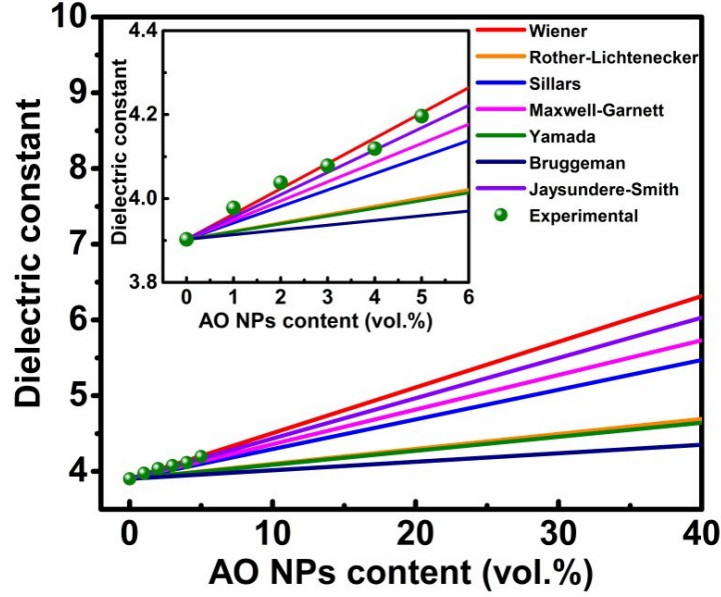**Fig. S5** Dielectric constant of AO NPs/PMMA single-layer nanocomposites with different concentrations of AO NPs fitted with classic two-component dielectric models (inset is the newly developed three-component interphase dielectric model and the illustration of the polymer-filler-interface components in the nanocomposites).

In this work, the classical two-component mathematical model used to calculate the dielectric constant of nanocomposites is as follows:

Wiener bounds model:[s11]

$$\varepsilon_{eff} = \varphi_f \varepsilon_f + \varphi_m \varepsilon_m \tag{S1}$$

Modified Rother−Lichtenecker model:[s12]

$$In\varepsilon_{eff} = In\varepsilon_m + \varphi_f(1 - \eta)In(\frac{\varepsilon_f}{\varepsilon_m}) \tag{S2}$$

Sillars model:[s13]

$$\varepsilon_{eff} = \varepsilon_m\left[1 + \frac{3\varphi_f(\varepsilon_f - \varepsilon_m)}{2\varepsilon_m + \varepsilon_f}\right] \tag{S3}$$

Maxwell-Garnett model:[s14-s16]

$$\varepsilon_{eff} = \varepsilon_m \left[1 + \frac{3\varphi_f(\varepsilon_f - \varepsilon_m)}{\varphi_m(\varepsilon_f - \varepsilon_m) + 3\varepsilon_m} \right]$$

(S4)

Yamada model:[s17,s18]

$$\varepsilon_{eff} = \varepsilon_m \left[1 + \frac{\eta \varphi_f(\varepsilon_f - \varepsilon_m)}{\eta \varepsilon_m + (1 - \varphi_f)(\varepsilon_f - \varepsilon_m)} \right]$$

(S5)

Bruggeman self-consistent effective medium approximation model:[s19]

$$\frac{\varepsilon_f - \varepsilon_{eff}}{\varepsilon_{eff}^{\frac{1}{3}}} = \frac{(1 - \varphi_f)(\varepsilon_f - \varepsilon_m)}{\varepsilon_m^{\frac{1}{3}}}$$

(S6)

Jaysundere-Smith model:[s20]

$$\varepsilon_{eff} = \frac{\varepsilon_m \varphi_m + \varepsilon_f \varphi_f \left[1 + 3\varphi_f \frac{\varepsilon_f - \varepsilon_m}{2\varepsilon_m + \varepsilon_f} \right]}{\varphi_m + \varphi_f \frac{3\varepsilon_m}{2\varepsilon_m + \varepsilon_f} \left[1 + 3\varphi_f \frac{\varepsilon_f - \varepsilon_m}{2\varepsilon_m + \varepsilon_f} \right]}$$

(S7)

where ε_{eff}, ε_f and ε_m are effective dielectric constant of nanocomposites, filler and polymer matrix, respectively; φ_m and φ_f are volume fractions of polymer matrix and fillers, η is a shaper factor.

Recently, three-component interphase dielectric model proposed by Wang et al. to calculate the dielectric constants of nanocomposites is briefly described as follows:[s21-s23]

$$K_c^\beta = \varphi_1 K_1^\beta + \varphi_2 K_2^\beta + \varphi_3 K_3^\beta$$

(S8)

where K_c, K_1, K_2 and K_3 are the K values of composite, polymer matrix, filler and interface, respectively; φ_1, φ_2 and φ_3 are volume fractions of polymer matrix, filler and interface, respectively; β is a filler dimension factor, for spherical fillers.

φ_3 can be determined from the multi-core model and written as:[s24]

$$\varphi_3 = \varphi_2 \left[\left(1 + \frac{2t}{d} \right)^3 - 1 \right] (1 - f), f = \left(\frac{6\varphi_2}{\pi} \right)^3$$

(S9)

where d is the diameter of filler and t is the thickness of interface, f is a general interphase overlap

probability function to evaluate the degrees of interface overlapping.

K_3 can be written as:

$$K_3^\beta = K_1^\beta + \varphi_f\left(K_2^\beta - K_1^\beta\right) + F(\varphi_2)K_1^\beta \qquad (S10)$$

where $F(\varphi_2)$ represents the degree of extra enhancement of K in interface, and can be written as:

$$F(\varphi_2) = 1 + \frac{T}{p + (\varphi_2/\varphi_0)^q} \qquad (S11)$$

Where $T = (K_2 + qK_1)(K_1)^{\frac{1}{2}}$, φ_0 is the filling ratio where maximum K_c is achieved, p and q are matrix-determined system factors (for dipolar linear polymer, $p=1$, $q=3$).
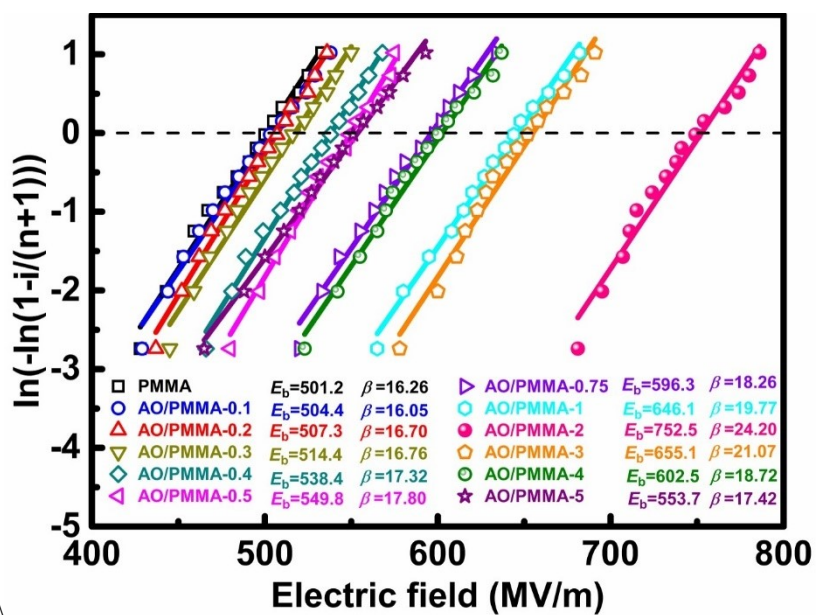
Fig. S6 Weibull breakdown strength of pristine PMMA and the PMMA single-layer nanocomposites with different contents of AO NPs.
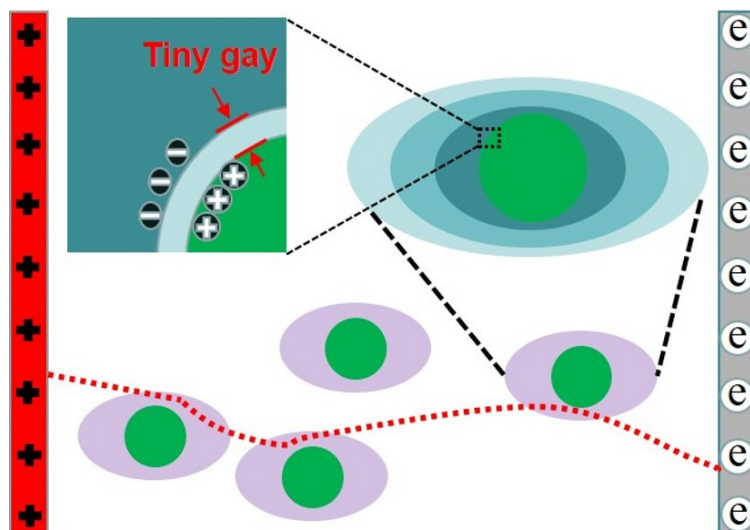
Fig. S7 Schematic image of breakdown paths for nanocomposites under the applied electrical field and the interface state.
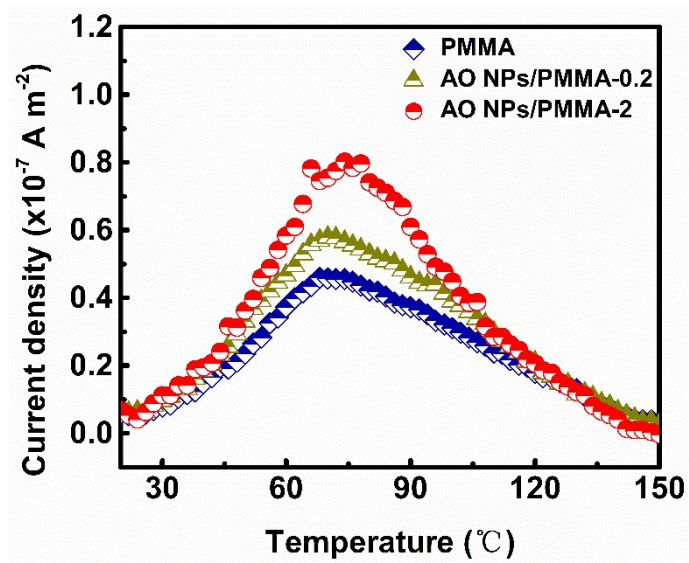
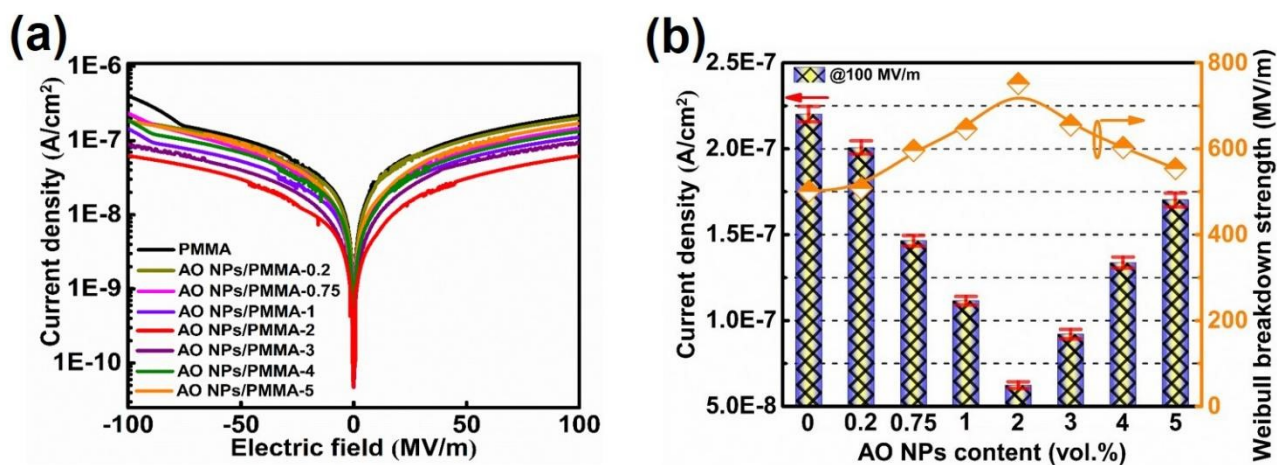**Fig. S8** TSDC spectra of PMMA, AO NPs/PMMA-0.2 and AO NPs/PMMA-2 composite films.

Fig. S9 (a) Leakage current density as a function of applied electric fields, (b) Weibull breakdown strength and leakage current density at 100 MV/m of pristine PMMA and the PMMA nanocomposites with different contents of AO NPs.
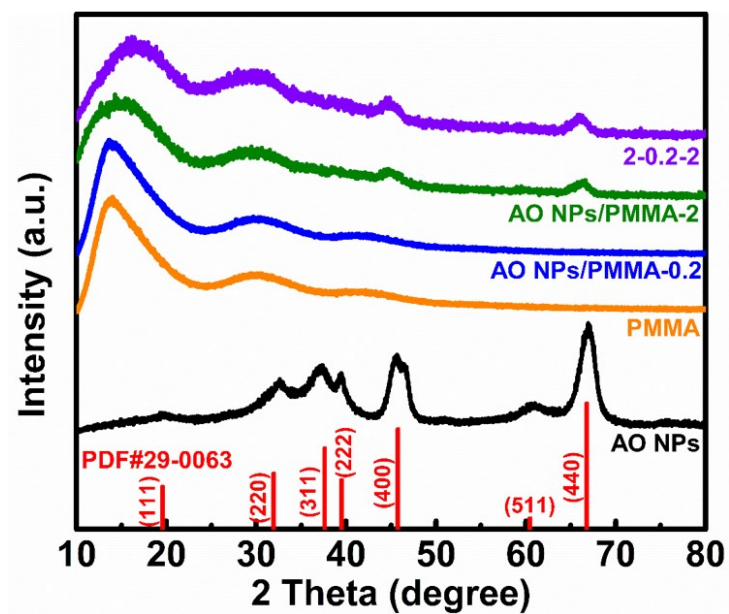
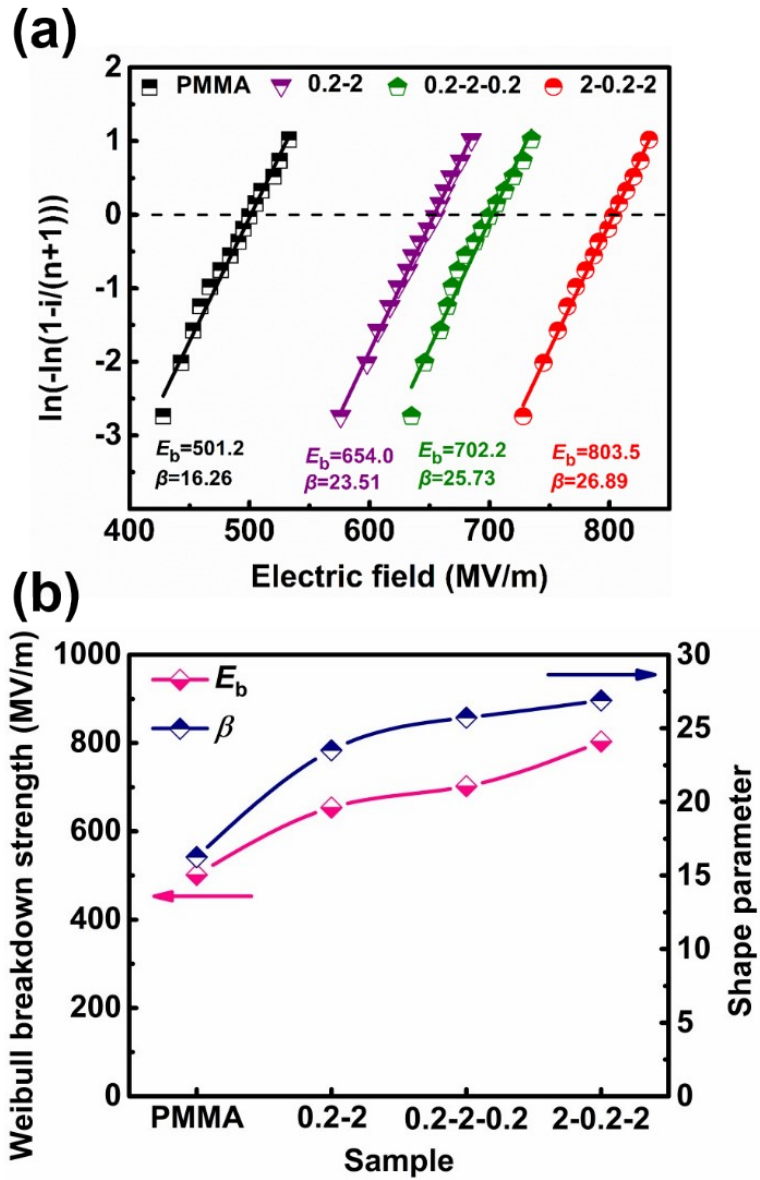**Fig. S10** XRD patterns of AO NPs, PMMA, AO/PMMA-0.2, AO/PMMA-2 and 2-0.2-2 composite films.

Fig. S11 (a) and (b) Characteristic breakdown strength and shape parameter of PMMA, 0.2-2, 0.2-2-0.2, and 2-0.2-2 multilayered composite films.
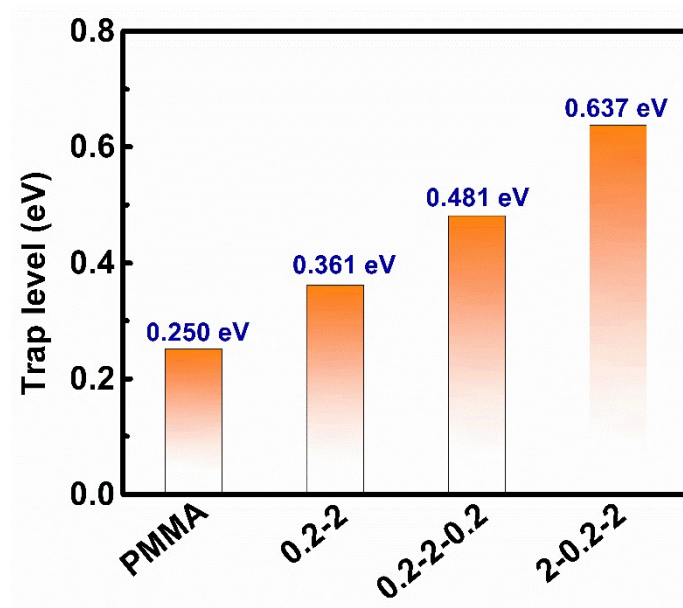
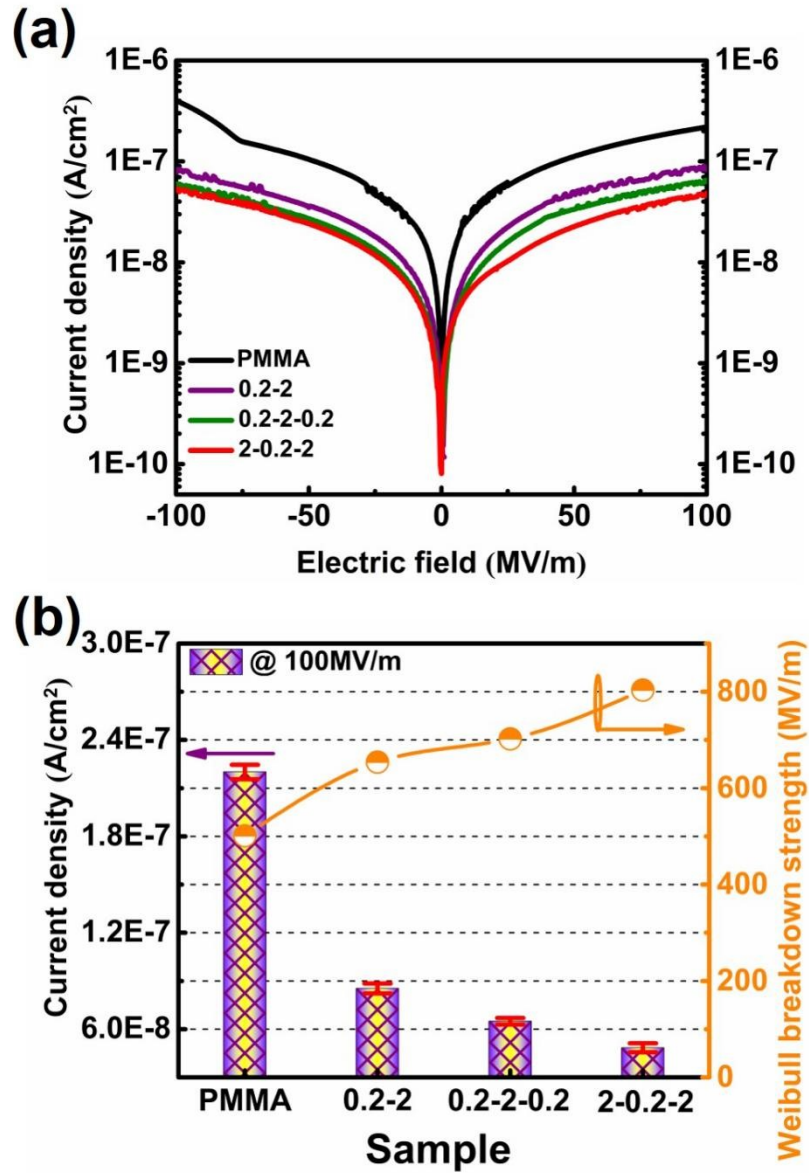**Fig. S12** The trap level of PMMA, 0.2-2, 0.2-2-0.2, 2-0.2-2 films.

Fig. S13 (a) Leakage current density as a function of applied electric fields; (b) Weibull breakdown strength and leakage current densities at 100 MV/m of PMMA, 0.2-2, 0.2-2-0.2, and 2-0.2-2 multilayered composite films.
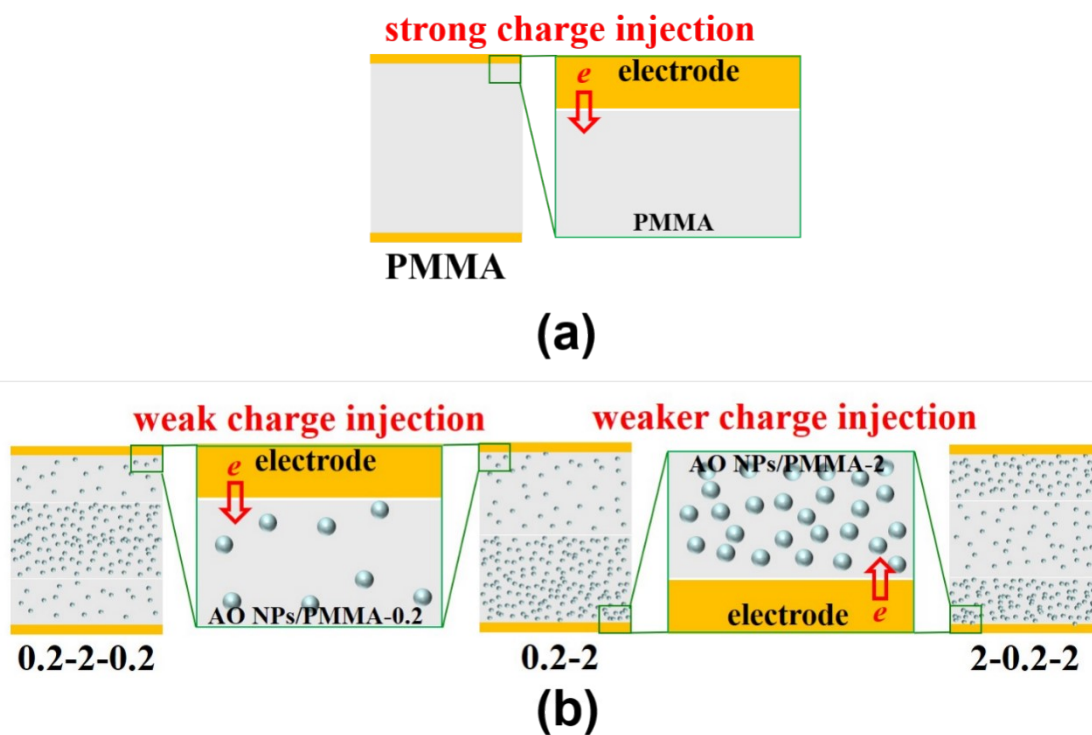
Fig. S14 Schematic representation of the metal/dielectric interface for, (a) PMMA, (b) 2-0.2-2, 0.2-2, and (c) 0.2-2-0.2 composite films.
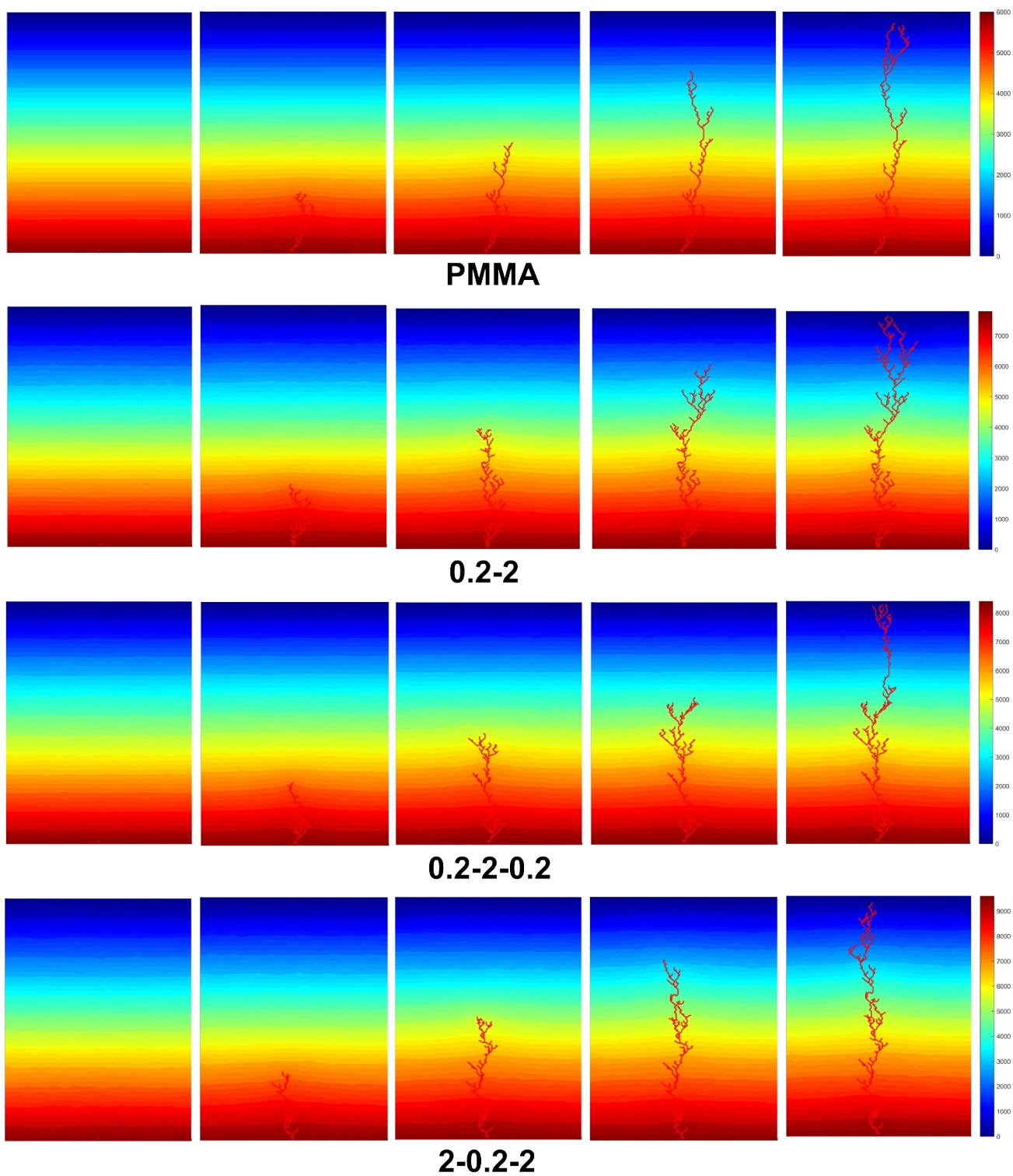
Fig. S15 The electric potential distribution and electrical trees evolution of PMMA, 0.2-2, 0.2-2-0.2 and 2-0.2-2 nanocomposites.
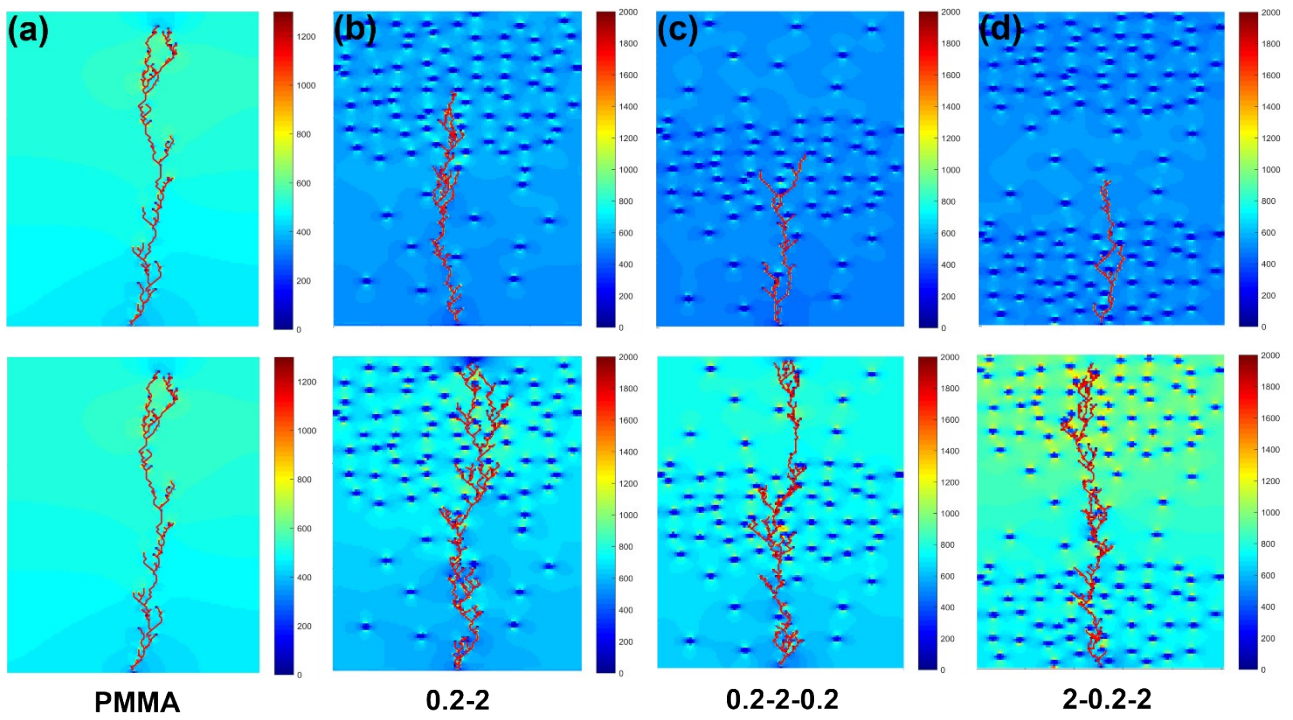
Fig. S16 Electric field distribution and electrical tree evolution of (a) PMMA, (b) 0.2-2 nanocomposite, (c) 0.2-2-0.2 nanocomposite, and (d) 2-0.2-2 nanocomposite at 500 MV/m (above) and maximum electric field (below).
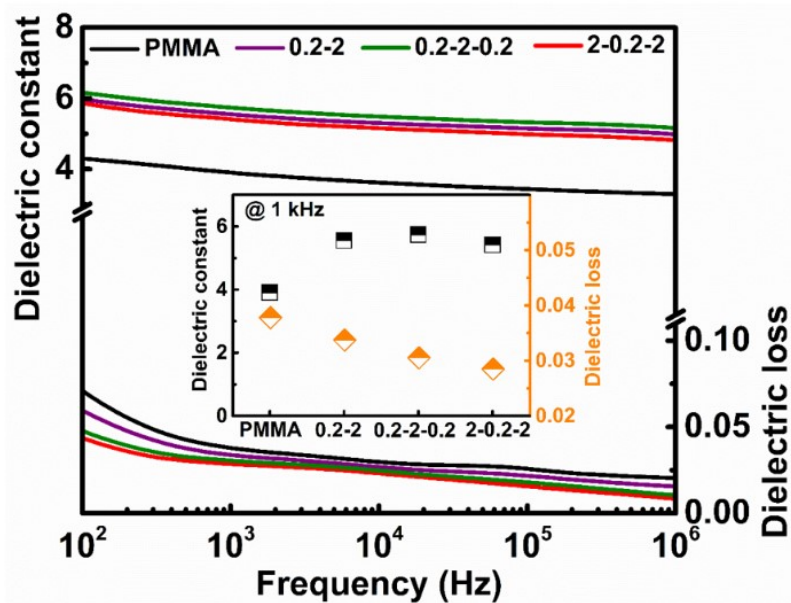
Fig. S17 Dielectric constant and dielectric loss as function of frequency (inset is the *K* at 1 kHz.) for

PMMA, 0.2-2, 0.2-2-0.2, and 2-0.2-2 nanocomposites.

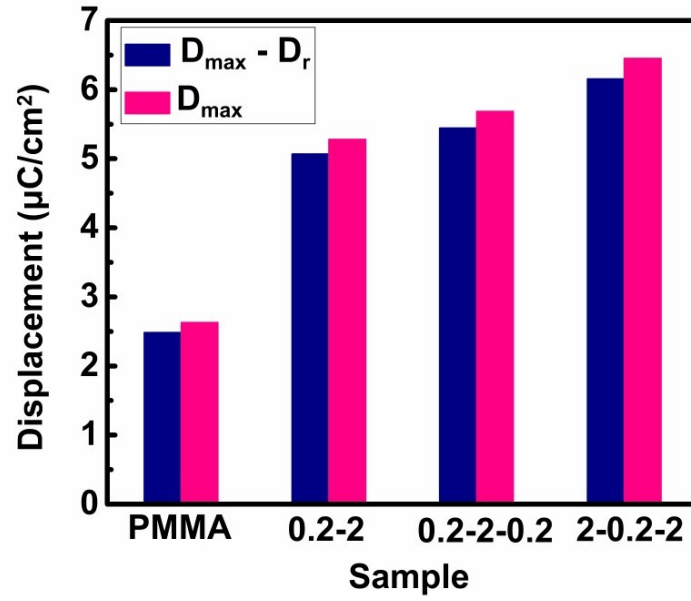**Fig. S18** $D_{\mathrm{max}} - D_{\mathrm{r}}$ and D_{max} of PMMA, 0.2-2, 0.2-2-0.2, and 2-0.2-2 multilayered composite films at the breakdown electric field.
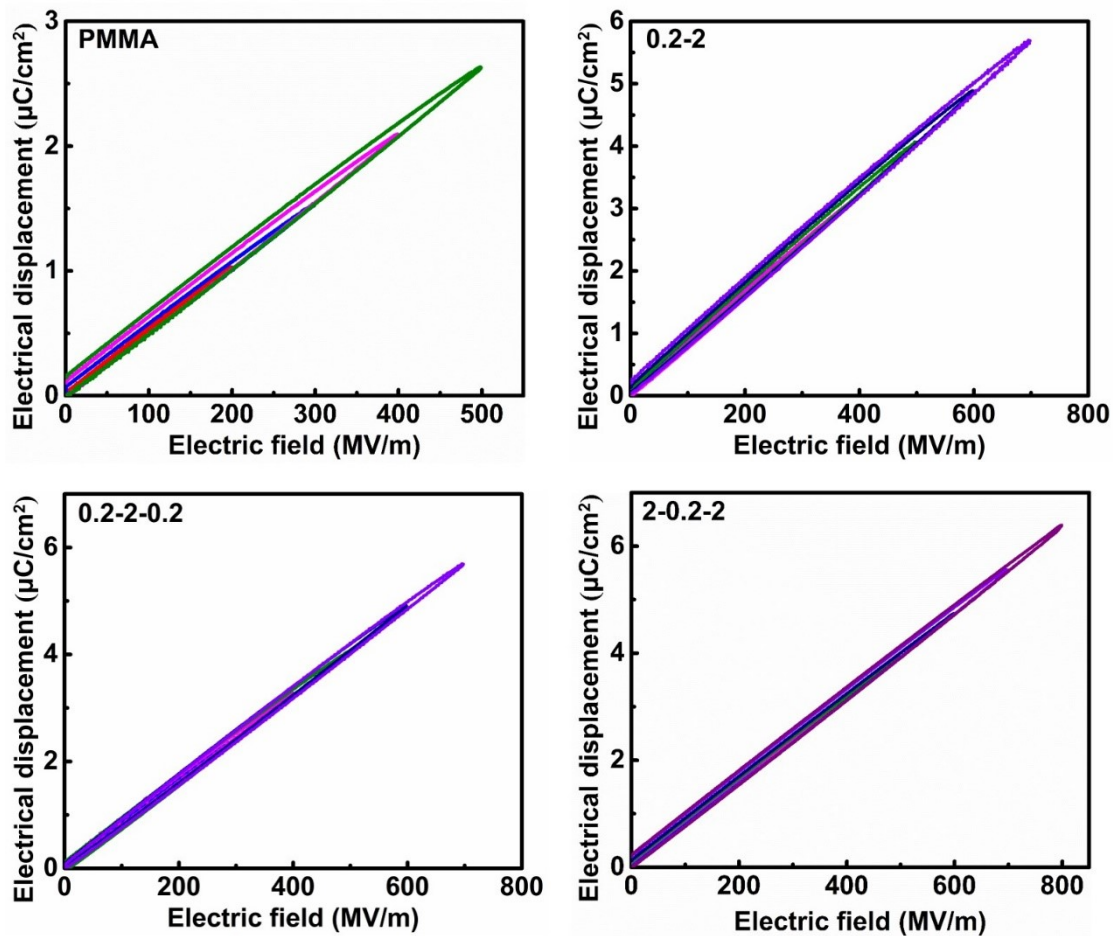
Fig. S19 *D−E* curves of PMMA, 0.2-2, 0.2-2-0.2, and 2-0.2-2 multilayered composite films.
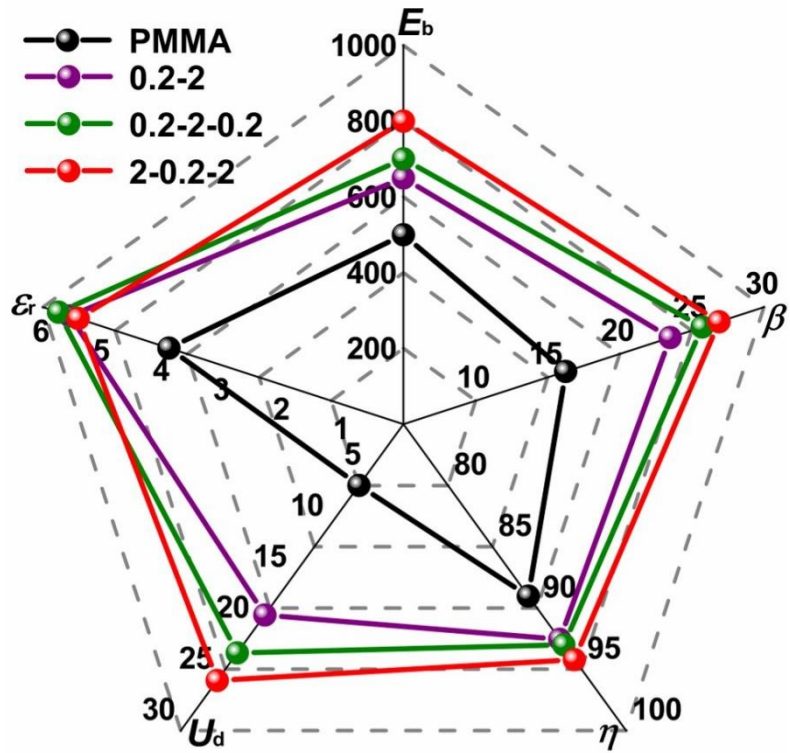
Fig. S20 Comparison of E_b, β, η, U_d and ε_r (at 1 kHz) of PMMA, 0.2-2, 0.2-2-0.2, and 2-0.2-2 multilayered composite films.
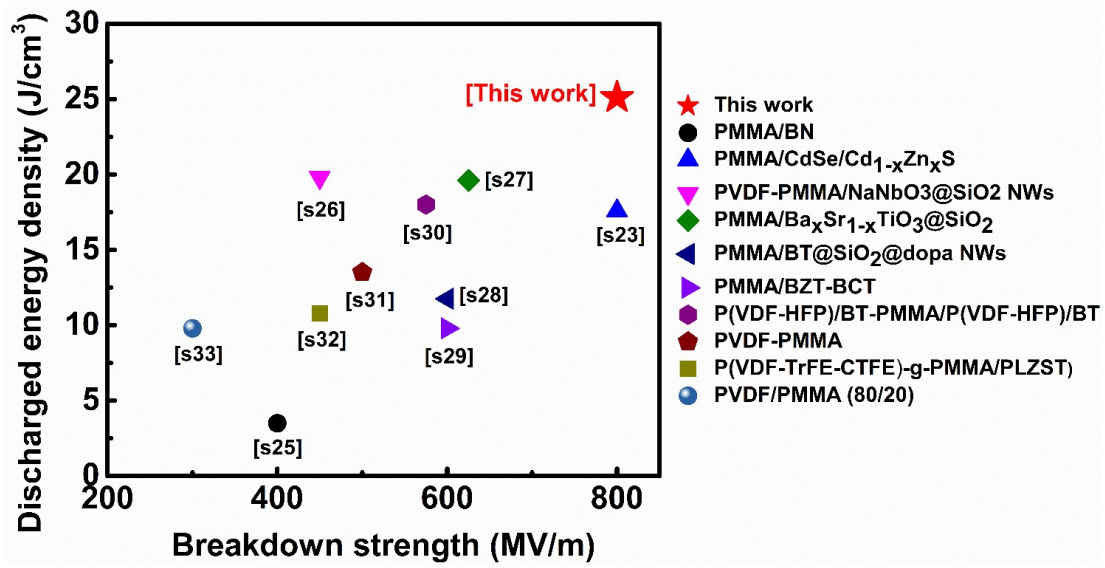
Fig. S21 Comparisons of the Weibull breakdown strengths and the corresponding maximum recoverable energy densities of PMMA-based nanocomposites. [s23, s25-s33]
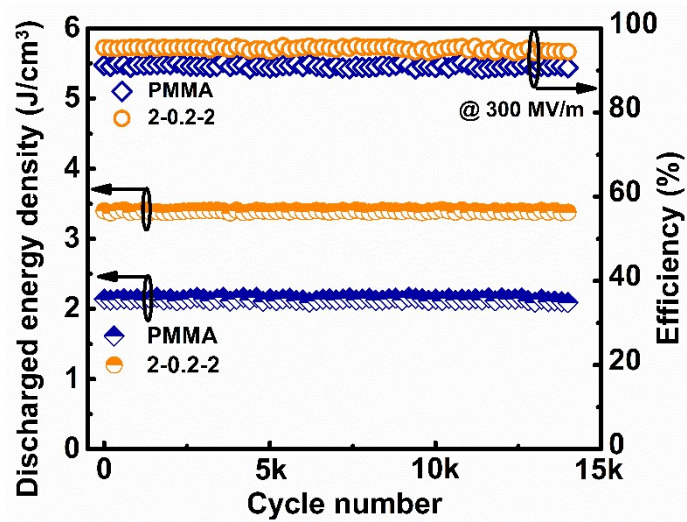
Fig. S22 The cyclic stability at 300MV/m of PMMA and 2-0.2-2 composite films.

Table S1 Comparison of key dielectric parameters achieved at the maximized U_d in this work and those reported in literatures.

Samples	$U_{d\,max}$ (J/cm^3) η (%) at E_b	U_d, $\eta \geq 90\%$ (J/cm^3)	Stability (cyclic number)	Ref.
P(VDF-HFP)-AO NPLs	21.6, 83.4, 697	0.2@50MV/m	>50,000	s34
P(VDF-HFP)-GLC	37.7, 71.2, 750	3.4@200MV/m	>50,000	s35
PVDF-BaTiO$_3$@BN	17.6, 58, 580	2.36@200MV/m	-	s36
BT@AS-MMT-P(VDF-HFP)	20, 84, 510	0.82@100MV/m	-	s37
P(VDF-TrFE-CFE)-BNNS	31.8, 72.7, 780	1.01@150MV/m	-	s38
PEI/BT-PVDF	8, 84.5, 600	4.4@450MV/m	>50,000	s39
PEI/HEnf	7.73, 88.7, 610	3.7@450MV/m	>50,000	s40
BZT/PEI-BN	17.9, 80.1, 730	6.2@400MV/m	-	s41
PEI/PEEU	7.80, 74.5, 710	7.2@650MV/m	>20,000	s42
PSBNP-co-PTNI$_{0.02}$	12.8, 88.7, 840	9.1@700MV/m	-	s43
2-0.2-2	25.1, 93.8, 800	25.1@800MV/m	>14,000	This Work

References

[s1] B. Xie, Q. Wang, Q. Zhang, Z. Liu, J. Lu, H. Zhang, S. Jiang, *ACS Appl. Mater. Interfaces* 2021, **13**, 27382.

[s2] T. Zhang, L. Yang, C. Zhang, Y. Feng, J. Wang, Z. Shen, Q. Chen, Q. Lei, Q. Chi, *Mater. Horiz.* 2022, **9**, 1273.

[s3] H. Li, L. Ren, D. Ai, Z. Han, Y. Liu, B. Yao, Q. Wang, *InfoMat* 2019, **2**, 389.

[s4] D. Ai, H. Li, Y. Zhou, L. Ren, Z. Han, B. Yao, W. Zhou, L. Zhao, J. Xu, Q. Wang, *Adv. Energy Mater.* 2020, **10**, 1903881.

[s5] Y. Li, J. Yin, Y. Feng, J. Li, H. Zhao, C. Zhu, D. Yue, Y. Liu, B. Su, X. Liu, *Chem. Eng. J.* 2022, **429**, 132228.

[s6] Z. Pan, L. Yao, J. Liu, X. Liu, F. Pi, J. Chen, B. Shen, J. Zhai, *J. Mater. Chem. C* 2019, **7**, 405.

[s7] X. Lu, X. Zou, J. Shen, L. Zhang, L. Jin, Z. Y. Cheng, *Nano Energy* 2020, **70**, 104551.

[s8] T. Zhang, X. Chen, Y. Thakur, B. Lu, Q. Zhang, J. Runt, Q. M. Zhang, *Sci. Adv.* 2020, **6**, eaax6622.

[s9] L. Li, Y. Zhou, Y. Liu, X. Chen, Z. Han, Q. Wang, *Appl. Phys. Lett.* 2022, **120**, 050502.

[s10] Y. Thakur, T. Zhang, C. Iacob, T. Yang, J. Bernholc, L. Q. Chen, J. Runt, Q. M. Zhang, *Nanoscale* 2017, **9**, 10992.

[s11] Z.-M. Dang, J.-K. Yuan, J.-W. Zha, T. Zhou, S.-T. Li, G.-H. Hu, *Prog. Mater. Sci.* 2012, **57**, 660.

[s12] Z. Ahmad, A. Prasad, K. Prasad, *Physica B Condens. Matter.* 2009, **404**, 3637.

[s13] R. W. Sillars, *J. Inst. Electr. Eng.* 1937, **80**, 378.

[s14] E. Tuncer, S. M. Gubański, B. Nettelblad, *J. Appl. Phys.* 2001, **89**, 8092.

[s15] J. M. Garnett, Philosophical Transactions of the Royal Society of London. Series A, *Containing Papers of a Mathematical or Physical Character* 1904, **203**, 385.

[s16] S. E. Skipetrov, *Phys. Rev. B* 1999, **60**, 12705.

[s17] T. Yamada, T. Ueda, T. Kitayama, *J. Appl. Phys.* 1982, **53**, 4328.

[s18] R. E. Newnham, D. P. Skinner, L. E. Cross, *Mater. Res. Bull.* 1978, **13**, 525.

[s19] V. D. Bruggeman, *Annalen Der Physik* 1935, **416**, 636.

[s20] N. Jayasundere, B. V. Smith, *J. Appl. Phys.* 1993, **73**, 2462.

[s21] L. Li, J. Cheng, Y. Cheng, T. Han, Y. Liu, Y. Zhou, G. Zhao, Y. Zhao, C. Xiong, L. Dong, Q. Wang, *Adv. Mater.* 2021, **33**, 2102392.

[s22] L. Li, Y. Zhou, Y. Liu, X. Chen, Z. Han, Q. Wang, *Appl. Phys. Lett.* 2022, **120**, 050502.

[s23] L. Li, J. Cheng, Y. Cheng, T. Han, Y. Liu, Y. Zhou, Z. Han, G. Zhao, Y. Zhao, C. Xiong, L. Dong, Q. Wang, *J. Mater. Chem. A* 2021, **9**, 23028.

[s24] T. Tanaka, M. Kozako, N. Fuse, Y. Ohki, *IEEE Trans. Dielectr. Electr. Insul.* 2005, **12**, 669.

[s25] F. Liu, Q. Li, Z. Li, Y. Liu, L. Dong, C. Xiong, Q. Wang, *Compos. Sci. Technol.* 2017, **142**, 139

[s26] Q. Sun, J. Wang, L. Zhang, P. Mao, S. Liu, L. He, F. Kang, R. Xue, *J. Mater. Chem. C* 2020, **8**, 7211.

[s27] C. Huang, L. Zhang, S. Liu, Y. Wang, N. Wang, Y. Deng, *Chem. Eng. J* 2021, **411**, 128585.

[s28] B. Xie, Q. Wang, Q. Zhang, Z. Liu, J. Lu, H. Zhang, S. Jiang, *ACS Appl. Mater. Interfaces,* 2021, **13**, 27382.

[s29] V. S. Puli, M. Ejaz, R. Elupula, M. Kothakonda, S. Adireddy, R. S. Katiyar, S. M. Grayson, D. B. Chrisey, *Polymer* 2016, **105**, 35.

[s30] Z. Li, Z. Shen, X. Yang, X. Zhu, Y. Zhou, L. Dong, C. Xiong, Q. Wang, *Compos. Sci. Technol.* 2021, **202**, 108591.

[s31] B. Luo, X. Wang, H. Wang, Z. Cai, L. Li, *Compos. Sci. Technol.* 2017, **151**, 94.

[s32] J. Wang Y. Xie, C. Chen, B. Peng, B. Zhang, Z. Zhang, *IET Nanodielectrics*, 2021, **4**, 171.

[s33] Y. Liu, J. Gao, Y. Wang, J. Zhou, L. Cao, Z. He, Y. Zhang, C. Tang, L. Zhong, *Macromol. Rapid. Commun.* 2019, **40**, 1900406.

[s34] H. Li, T. Yang, Y. Zhou, D. Ai, B. Yao, Y. Liu, L. Li, L. Chen, Q. Wang, *Adv. Funct. Mater.* 2021, **31**, 2006739.

[s35] R. Wang, H. Xu, S. Cheng, J. Liang, B. Gou, J. Zhou, J. Fu, C. Xiong, J. He, Q. Li, *Energy Storage Mater.* 2022, **49**, 339.

[s36] S. Luo, J. Yu, S. Yu, R. Sun, L. Cao, W. Liao, C. Wong, *Adv. Energy. Mater.* 2019, **9**, 1803204.

[s37] B. Luo, Z. Shen, Z. Cai, E. Tian, Y. Yao, B. Li, A. Kursumovic, J. L. MacManus-Driscoll, L. Li, L. Q. Chen, X. Wang, *Adv. Funct. Mater.* 2020, **31**, 2007994.

[s38] J. Chen, Z. Shen, Q. Kang, X. Qian, S. Li, P. Jiang, X. Huang, *Sci. Bull.* 2022, **67**, 609.

[s39] B. Zhang, X. Chen, W. Wu, A. Khesro, P. Liu, M. Mao, K. Song, R. Sun, D. Wang, *Chem. Engineer. J.* 2022, **446**, 136926.

[s40] L. Dou, B. Yang, S. Lan, Y. Liu, Y. Liu, C. Nan, Y. Lin, *Adv. Energy Mater.* 2023, **13**, 2203925.

[s41] H. Liu, W. Zhu, Q. Mao, B. Peng, Y. Xu, G. Dong, B. Chen, R. Peng, Y. Zhao, Z. Zhou, S. Yang, H. Huang, M. Liu, *Adv. Mater.* 2023, **35**, 2300962.

[s42] S. Ding, Z. Bao, Y. Wang, Z. Dai, J. Jia, S. Shen, Y. Yin, X. Li, *J. Power Sources* 2023, **570**, 233053.

[s43] J. Chen, Y. Zhou, X. Huang, C. Yu, D. Han, A. Wang, Y. Zhu, K. Shi, Q. Kang, P. Li, P. Jiang, X. Qian, H. Bao, S. Li, G. Wu, X. Zhu, Q. Wang, *Nature* 2023, **615**, 62.